Boundary Extraction Enhanced Distorted Born Iterative Method for Microwave Mammography

Kazuki Noritake and Shouhei Kidera, *Member, IEEE*

***Abstract*—This letter focuses on improving the accuracy of the distorted Born iterative method (DBIM)-based inverse scattering algorithm, using accurate boundary extraction in microwave mammography. It is well known that the accuracy of inverse scattering algorithms depends on the initial estimate of the region of interest (ROI). The Envelope algorithm is one of the promising algorithms for accurate ROI estimation. However, in the near-field breast imaging scenario, the coupling effect between an antenna and the breast surface incurs a nonnegligible error for Envelope-based boundary extraction, which is mainly caused by the mismatching between the reference and measured waveforms. To address this problem, this letter introduces the finite-difference time-domain-based waveform reconstruction for improving the accuracy of DBIM-based microwave imaging. The two-dimensional numerical simulations, using realistic breast phantoms derived from magnetic resonance images, demonstrate that our proposed algorithm remarkably enhances the accuracy of the DBIM, even in highly heterogeneous cases.**

***Index Terms*—Distorted born iterative method (DBIM), envelope-based boundary extraction, finite-difference time-domain (FDTD)-based waveform correction, microwave mammography.**

I. Introduction

ACCORDING to the World Cancer Research Fund, breast cancer is the most widely diagnosed cancer in women. Although X-ray mammography is the commonly used screening technique for the detection of malignant tumors, this method can harm cells and requires the breast to be highly compressed. These drawbacks result in low rates of successful examination, particularly in young women. Magnetic resonance imaging (MRI) is one of the promising options offering safe and high-spatial-resolution imaging. Nevertheless, it requires some rather large-scale equipment for both electric and magnetic shielding. Microwave mammography is one of the most promising alternative tools, which has some advantages over the X-ray-based modality. The equipment is portable and inexpensive, and the measurement is not harmful.

The physical basis of microwave mammography is the significant contrast between the dielectric properties of normal tissues (adipose dominant) and malignant tumors, which has been demonstrated extensively in the literature [1]. Microwave imaging methods have been divided into the following two categories. One is a confocal algorithm, e.g., beamforming or modified delay-and-sum [2], and the other is an inverse scattering algorithm, e.g., the extended Born approximation [3] or the distorted Born iterative method (DBIM) [4]. This letter focuses on the DBIM algorithm, which is applicable to highly heterogeneous and highly contrasted media. However, many reports have revealed that the DBIM-based algorithm faces the problem of severe sensitivity to an initial estimate of the dielectric property map and a region of interest (ROI), namely, the outer breast boundary [5]. While laser-based surface measurements have been developed [6], there are difficulties for adjusting the microwave and laser sensors, and a simultaneous measurement for surface shape and tumor is indispensable for accurate image reconstruction. There are a number of surface shape estimation algorithms in medical imaging issue, such as the exploitation of the resonant frequency shift between an antenna and a skin [7]. As a representative ROI estimation algorithm for breast media, the Envelope method is one of the most promising options [8]. The similar algorithm specifying the breast surface, referred to as breast boundary identification, has also been also introduced in the literature [9], [10]. The key point of accurate boundary extraction by the Envelope-based method is the accuracy for time-delay estimations from the antennas to the breast surface. However, due to the coupling effect between the antenna and the skin surface, a skin reflection waveform often mismatches the reference waveform, which leads to a nonnegligible error for range estimation based on waveform matching-based filter, e.g., a matched filter.

To address the above-mentioned issue, this letter proposes an accuracy-enhanced Envelope method that uses the finite-difference time-domain (FDTD) recovered signal, which we have recently proposed [11]. The range error is directly compensated by assessing the time shift between the observed and FDTD recovered signal, where a frequency dependence of surface reflection can be included, which was not accurately modeled in [10]. The proposed method incorporates the FDTD-enhanced Envelope method to provide the initial ROI into the DBIM process. The results of the two-dimensional (2-D) FDTD-based numerical simulations of numerical phantoms derived from MRI demonstrate that the proposed algorithm greatly enhances the convergence speed and reconstruction accuracy of DBIM for highly heterogeneous breast media.

II. Observation Model

Fig. 1 shows the observation model. An array of multiple transmitters and receivers is located along the circumference curve, which surrounds an object area. The breast medium is composed of skin, adipose, and fibro-glandular tissues, each of which are lossy, dispersive, and have isotropic dielectric properties. $E^{\mathrm{scat}}(\boldsymbol{r}_{\mathrm{t}}, \boldsymbol{r}_{\mathrm{r}}; t)$ denotes the observed scattered electric field

Manuscript received December 10, 2018; revised January 21, 2019; accepted February 26, 2019. Date of publication March 1, 2019; date of current version April 5, 2019. This work was supported by the MIC/SCOPE #162103102. *(Corresponding author: Shouhei Kidera.)*

The authors are with the Graduate School of Informatics and Engineering, The University of Electro-Communications, Tokyo 182-8585, Japan (e-mail: kidera@uec.ac.jp; noritake.kazuki@ems.cei.uec.ac.jp).

Digital Object Identifier 10.1109/LAWP.2019.2902351

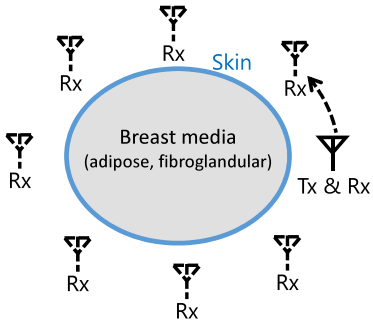

Fig. 1. Observation model.

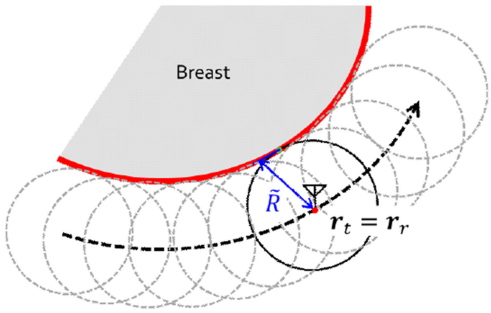

Fig. 2. Envelope-based boundary reconstruction.

at time t, where $\boldsymbol{r}_{\rm t}$ and $\boldsymbol{r}_{\rm r}$ are the locations of the transmitter and receiver, respectively.

III. Reconstruction Method

A. Distorted Born Iterative Method

The complex permittivity map in breast media can be reconstructed by solving the Helmholtz-type integral equation. Focusing on the scattered field $E^{\rm scat}(\boldsymbol{r})$, observed at the location $\boldsymbol{r}$, the following integral equation holds:

$$E^{\rm scat}(\boldsymbol{r}) \equiv E^{\rm total}(\boldsymbol{r}) - E^{\rm in}(\boldsymbol{r}) = \omega^2\mu \int_V G_0(\boldsymbol{r},\boldsymbol{r}')E^{\rm total}(\boldsymbol{r}')o(\boldsymbol{r}'){\rm d}\boldsymbol{r}' \quad (1)$$

where V is the ROI area, $E^{\rm scat}(\boldsymbol{r})$ and $E^{\rm total}(\boldsymbol{r})$ are the scattered and total electric fields, respectively, $E^{\rm in}(\boldsymbol{r})$ is the incident field in the presence of the background complex relative permittivity denoted as $\epsilon_0(\boldsymbol{r})$, $G_0(\boldsymbol{r},\boldsymbol{r}')$ is Green's function assuming the background medium, and $o(\boldsymbol{r}) = \epsilon(\boldsymbol{r}) - \epsilon_0(\boldsymbol{r})$ denotes the object function, where $\epsilon(\boldsymbol{r})$ is an actual complex relative permittivity. The inverse scattering algorithm solves the object function $o(\boldsymbol{r})$ using the recorded scattered field $E^{\rm scat}(\boldsymbol{r})$. Here, assuming that $\Delta o(\boldsymbol{r})$ is sufficiently small, the difference between the true and assumed (or estimated) background media of the total field as $\Delta E^{\rm total}$ is approximated as

$$\Delta E^{\rm total}(\boldsymbol{r}) \equiv E^{\rm total}(\boldsymbol{r}) - E_{\rm b}^{\rm total}(\boldsymbol{r}) \simeq \omega^2\mu \int_V G_{\rm b}(\boldsymbol{r},\boldsymbol{r}')E_{\rm b}^{\rm total}(\boldsymbol{r})\Delta o(\boldsymbol{r}'){\rm d}\boldsymbol{r}' \quad (2)$$

where $G_{\rm b}(\boldsymbol{r},\boldsymbol{r}')$ is the Green's function of the background medium, and $\Delta o(\boldsymbol{r}) = o(\boldsymbol{r}) - o_{\rm b}(\boldsymbol{r})$, where $o_{\rm b}(\boldsymbol{r})$ is the object function of background. DBIM sequentially updates $o_{\rm b}(\boldsymbol{r})$, $G_{\rm b}(\boldsymbol{r},\boldsymbol{r}')$, and $E_{\rm b}^{\rm total}(\boldsymbol{r})$ to minimize $|\Delta E^{\rm total}(\boldsymbol{r})|^2$. For dispersive media, (e.g., breast material), each parameter in the assumed dispersive model (e.g. the Debye model) is updated using multiple frequency data [4]. While DBIM has been shown to accurately reconstruct the dielectric map even in highly heterogeneous cases, the iterative procedure requires an accurate initial estimate of the ROI boundary and its dielectric property.

B. FDTD-Enhanced Envelope Method for ROI Boundary Extraction in DBIM

To address the above-mentioned shortcoming of the DBIM method, we introduce an Envelope-based ROI boundary extraction [8] based on the following simple principle: An object's outer boundary can be expressed as an envelope of circles (or ellipses in a bistatic case), in which the center is the antenna location and the radius is the measured range between the antenna and the breast surface. Fig. 2 shows the principle of this Envelope-based method for a monostatic case (i.e., $\boldsymbol{r}_{\rm t} = \boldsymbol{r}_{\rm r}$). Here, the distance to the skin surface ($\hat{R}(\boldsymbol{r}_{\rm t},\boldsymbol{r}_{\rm r})$) is measured by the local maximum of the filter (e.g., matched filter) output using a specific reference signal $E^{\rm ref}(t)$, which is usually measured at the far-field case. The Envelope method does not require any optimization process for surface reconstruction, however, its accuracy depends on the accuracy of the measured range as $\hat{R}(\boldsymbol{r}_{\rm t},\boldsymbol{r}_{\rm r})$. The accuracy of range extraction depends on the similarity in waveforms between the observed and assumed reference signals. However, in most cases, the antennas and the breast surface are closely located within the central wavelength of the transmitted pulse. Thus, for near-field observations, the observed waveform is deformed with respect to the assumed reference waveform as a result of the coupling effect.

To enhance the accuracy of breast surface estimation, this letter introduces direct range compensation using the FDTD-recovered waveform. In this method, the reference signal is updated by the FDTD-based forward solver based on a prior estimation of the skin surface derived from the Envelope method. Since the FDTD-recovered signal (denoted as $\tilde{E}^{\rm scat}(\boldsymbol{r}_{\rm t},\boldsymbol{r}_r;t)$), includes the coupling effect between the skin and the antennas, it is expected to enhance the accuracy of range estimation by compensating for the above-mentioned waveform mismatch. The proposed method updates the range as

$$\tilde{R}(\boldsymbol{r}_{\rm t},\boldsymbol{r}_{\rm r}) = \hat{R}(\boldsymbol{r}_{\rm t},\boldsymbol{r}_{\rm r}) + {\rm c}\Delta\tau(\boldsymbol{r}_{\rm t},\boldsymbol{r}_{\rm r})/2 \quad (3)$$

where c is the speed of light in air, and $\Delta\tau(\boldsymbol{r}_{\rm t},\boldsymbol{r}_{\rm r})$ is calculated as

$$\Delta\tau(\boldsymbol{r}_{\rm t},\boldsymbol{r}_{\rm r}) = \arg\max_{\tau}\left[E^{\rm scat}(\boldsymbol{r}_{\rm t},\boldsymbol{r}_{\rm r};t) \star \tilde{E}^{\rm scat}(\boldsymbol{r}_{\rm t},\boldsymbol{r}_{\rm r};t)\right](\tau) \quad (4)$$

where $\star$ denotes the cross-correlation operator. Note that the optimization problem in (4) is simplified as peak-search processing. Since the updated reference waveform $\tilde{E}^{\rm scat}(\boldsymbol{r}_{\rm t},\boldsymbol{r}_{\rm r};t)$ includes the coupling and near-field effects, the similarity between the observed and reference waveforms is improved, which enhances the accuracy for the range compensation. Furthermore, it is expected that the boundary estimation performance of the Envelope method will also be upgraded by using the compensated ranges denoted as $\tilde{R}(\boldsymbol{r}_{\rm t},\boldsymbol{r}_{\rm r})$. Fig. 3 shows the flowchart of the proposed method. Note that the ROI updating process and the DBIM iteration sequences are completely separated in the proposed algorithm.

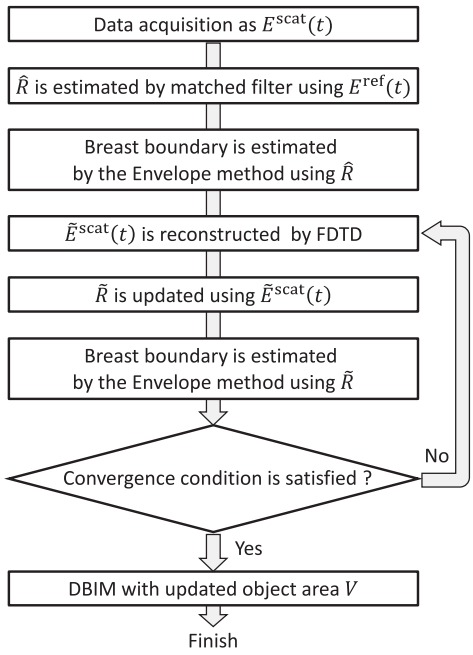

Fig. 3. Flowchart of the proposed method.

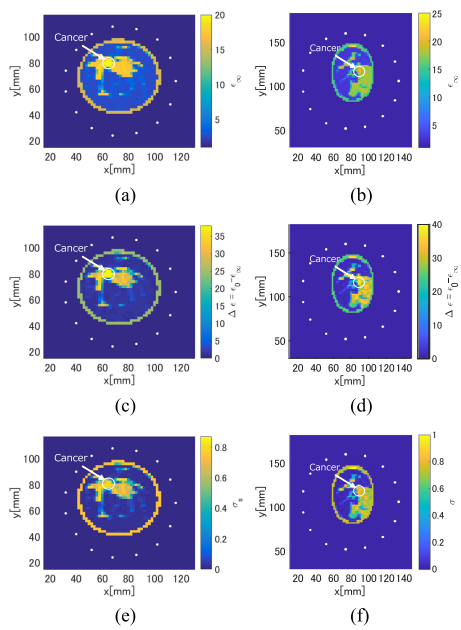

Fig. 4. Maps of the Debye parameters in Class-3 phantom (a): $\epsilon_\infty(\boldsymbol{r})$, (c) $\Delta\epsilon(\boldsymbol{r})$, and (e) $\sigma_s(\boldsymbol{r})$ and Class-4 phantom (b): $\epsilon_\infty(\boldsymbol{r})$, (d) $\Delta\epsilon(\boldsymbol{r})$ and (f) $\sigma_s(\boldsymbol{r})$.

IV. Numerical Tests

This section describes numerical tests of simulated array measurements of realistic breast phantoms derived from MRI scans of healthy women [12]. The tests included Class-3 (heterogeneously dense) and Class-4 (very dense) phantoms. The frequency-dependent complex permittivities of the breast phantoms were modeled using the single-pole Debye model, formulated as $\epsilon = \epsilon_\infty + \frac{\Delta\epsilon}{1+j\omega\tau} + \frac{\sigma}{j\omega\epsilon_0}$, the accuracy of which has been demonstrated on a number of real breast specimens [1]. Fig. 4 illustrates the maps of the Debye parameters ϵ_∞, $\Delta\epsilon$, and σ_s for Class-3 and -4 phantoms.

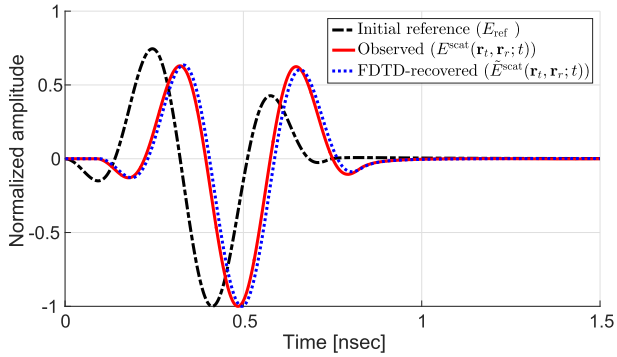

Fig. 5. Comparison of waveforms of the observed signal (red solid), initial reference signal (black broken), and FDTD-recovered signal (blue dotted).

TABLE I
Errors in Estimation (Err_V), Using the Envelope Method

	NOI for waveform compensations		
	0	1	2
Class 3	31.0%	11.8%	5.8%
Class 4	21.2%	9.2%	4.3%

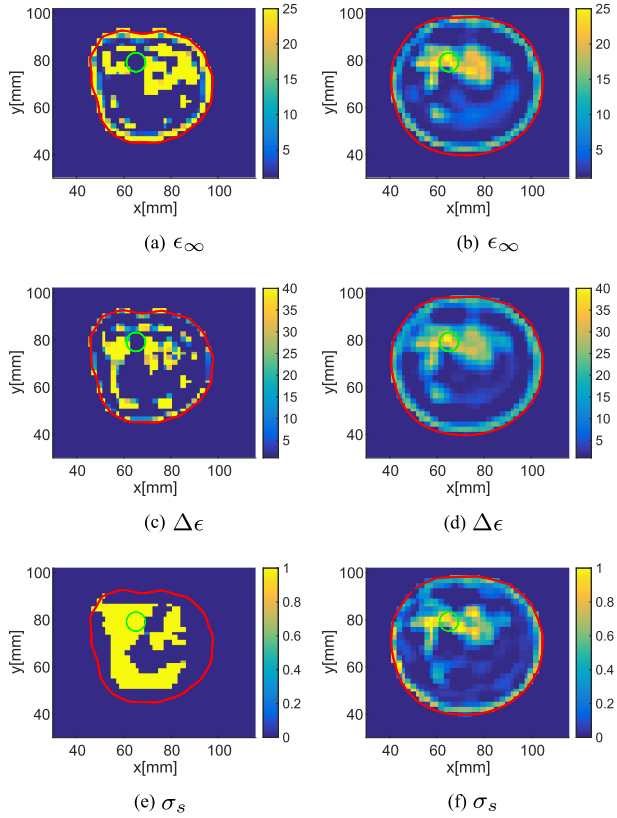

Fig. 6. DBIM reconstruction results for Class-3 phantom (red line shows boundary estimated by Envelope method). (a), (c), and (e) ROI is determined by the Envelope without range compensation. (b), (d), and (f) ROI is determined by the Envelope with range compensation (NOI is 2).

Both maps include 6 mm × 8 mm size tumors, whose Debye parameters are set as $\epsilon_\infty = 20$, $\Delta\epsilon = 38$, and $\sigma_s = 0.8$ S/m. Note that the average values of the Debye parameters for the proximity area around the tumors (predominantly fibro-glandular tissue) are estimated as $(\epsilon_\infty, \Delta\epsilon, \sigma_s) = (15.0, 23.4, 0.537\ \mathrm{S/m})$ in the case of Class 3, and $(\epsilon_\infty, \Delta\epsilon, \sigma_s) = (16.4, 26.7, 0.617\ \mathrm{S/m})$ in the case of Class 4.

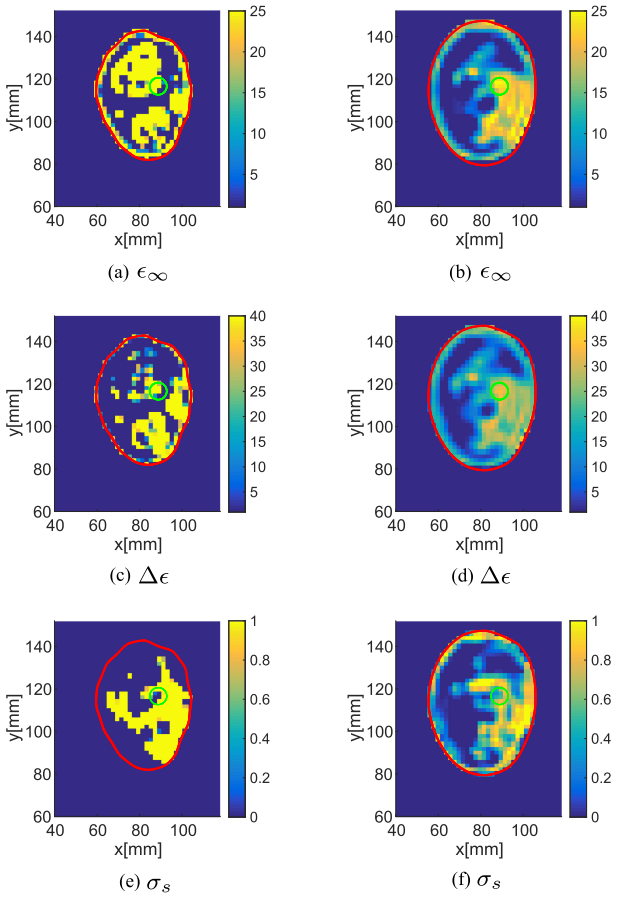

Fig. 7. DBIM reconstruction results for Class-4 phantom (red line shows boundary estimated by Envelope method). (a), (c), and (e) ROI is determined by the Envelope without range compensation. (b), (d), and (f) ROI is determined by the Envelope with range compensation (NOI is 2).

The transmitting signal formed a raised-cosine modulated pulse with a central frequency of 2.45 GHz and a bandwidth of 2.7 GHz. The number of antennas is 15, and all combination data from the transmitting and receiving antennas are processed in the DBIM. The scattered electric field is calculated by the FDTD method with the single-pole Debye model (in-house code provided by the cross-disciplinary electromagnetics laboratory, the University of Wisconsin–Madison). Transverse magnetic mode wave is assumed in the 2-D problem. The cell size of the FDTD is 2 mm. The conjugate gradient for least-squares method under l_2 norm regularization is used to update the DBIM with 20 being the maximum number of iterations with convergence check, which has been empirically determined by investigating several cases.

Fig. 5 compares the waveforms of the observed signal, the initial reference signal, and the FDTD-recovered signal at the specific observation point, assuming a Class-2 phantom. Fig. 5 demonstrates that the similarity between $E^{\mathrm{scat}}(t)$ and $\tilde{E}^{\mathrm{scat}}(t)$ is improved compared to that between $E^{\mathrm{scat}}(t)$ and $E^{\mathrm{ref}}(t)$. Table I summarizes the error in the boundary estimation of breast media in each number of iteration (NOI), defined as

$$\mathrm{Err}_V = \left| \int_{V_{\mathrm{true}}} \mathrm{d}\boldsymbol{r} - \int_{\hat{V}} \mathrm{d}\boldsymbol{r} \right| \Big/ \left| \int_{V_{\mathrm{true}}} \mathrm{d}\boldsymbol{r} \right| \qquad (5)$$

TABLE II
NRMSEs USING FDTD BASED WAVEFORM COMPENSATIONS FOR EACH DEBYE PARAMETERS AT CLASS-3 AND CLASS-4

	Class 3			Class 4		
NOI	ϵ_∞	$\Delta\epsilon$	σ_s	ϵ_∞	$\Delta\epsilon$	σ_s
0	2.013	2.181	2.580	1.500	1.436	1.580
1	1.578	1.818	2.095	1.115	1.071	1.417
2	0.436	0.594	0.712	0.409	0.466	0.704
ROI:Given	0.395	0.557	0.585	0.446	0.448	0.578

where V_{true} and $\hat{V}$ are the actual area of the object and the area estimated using the Envelope method, respectively. The errors in Table I verify that the proposed method considerably enhanced the accuracy of the surface shape estimation for Class-3 and -4 phantoms. It has been confirmed that the three or more iterations for waveform compensations would not improve the results significantly, which indicates that the coupling effect and shape dependence of the reflection signal is largely compensated by the first FDTD updating.

Figs. 6 and 7 show the DBIM reconstruction results obtained using the initial object boundary estimated by the Envelope method for each NOI of range compensations for Class-3 and Class-4 phantoms, respectively. The reconstruction accuracy of DBIM largely depends on the accuracy of the boundary estimation. Figs. 6 and 7 demonstrate that the proposed method successfully enhanced the accuracy of the boundary estimation and thereby enhanced the accuracy of the DBIM reconstruction. In this letter, for quantitative analysis, the normalized root-mean-square error (NRMSE) in the reconstruction for each Debye parameter is investigated as follows. Table II summarizes the NRMSEs for each parameter in the Class-3 and Class-4 phantoms. These results demonstrate that the enhanced-accuracy boundary extraction significantly accelerated the convergence speed.

V. CONCLUSION

This letter has introduced an enhanced-accuracy boundary extraction method that increases the convergence efficiency of the DBIM algorithm. In this method, the accuracy of Envelope-based boundary extraction is enhanced using the FDTD-recovered reference signal. Numerical tests with realistic breast phantoms of highly heterogeneous media demonstrated that the proposed method significantly enhances the accuracy and convergence speed of DBIM-based dielectric map reconstruction. In the numerical results, the DBIM-based optimization might reach a false solution, given the high contrast between the cancer and background media. The second-order approximation [13] or the quadratic distorted approach [14] should be considered to resolve the above-mentioned problem. Furthermore, a multistatic or bistatic model has the potential to enhance the accuracy of the Envelope-based breast surface reconstruction, as demonstrated [15], where its computational complexity is almost on the same level as that of the monostatic approach. Thus, in the case of a sparser array arrangement, which should be assumed in the 3-D model, the above extension should be considered because it provides more information about the breast surface, especially for an interpolation effect, than that provided by the monostatic model.

REFERENCES

[1] M. Lazebnik *et al.*, "A large-scale study of the ultrawideband microwave dielectric properties of normal, benign and malignant breast tissues obtained from cancer surgeries," *Phys. Med. Biol.* vol. 52, pp. 6093–2093 2007.

[2] D. Byrne, M. Sarafianou, and I. J. Craddock, "Compound radar approach for breast imaging," *IEEE Trans. Biomed. Eng.*, vol. 64, no. 1, pp. 40–51, Jan. 2017.

[3] Q. H. Liu *et al.*, "Active microwave imaging. I. 2-D forward and inverse scattering methods," *IEEE Trans. Microw. Theory Techn.*, vol. 50, no. 1, pp. 123–133, Jan. 2002.

[4] J. D. Shea *et al.*, "Three-dimensional microwave imaging of realistic numerical breast phantoms via a multiple-frequency inverse scattering technique," *Amer. Assoc. Phys. Med.*, vol. 37, no. 8, pp. 4210–4226, Aug. 2010.

[5] F. Gao, B. D. Van Veen, and S. C. Hagness, "Sensitivity of the distorted Born iterative method to the initial guess in microwave breast imaging," *IEEE Trans. Antennas Propag.*, vol. 63, no. 8, pp. 3540–3547, Aug. 2015.

[6] T. C. Williams *et al.*, "Laser surface estimation for microwave breast imaging systems," *IEEE Trans. Biomed. Eng.*, vol. 58, no. 5, pp. 1193–1199, May 2011.

[7] A. Zamani, S. A. Rezaeieh, K. S. Bialkowski, and A. M. Abbosh, "Boundary estimation of imaged object in microwave medical imaging using antenna resonant frequency shift," *IEEE Trans. Antennas Propag.*, vol. 66, no. 2, pp. 927–936, Feb. 2018.

[8] S. Kidera, T. Sakamoto, and T. Sato, "A robust and fast imaging algorithm with an envelope of circles for UWB pulse radars," *IEICE Trans. Commun.*, vol. E90-B, no. 7, pp. 1801–1809, Jul. 2007.

[9] D. W. Winters, J. D. Shea, E. L. Madsen, G. R. Frank, B. D. Van Veen, and S. C. Hagness, "Estimating the breast surface using UWB microwave monostatic backscatter measurements," *IEEE Trans. Biomed. Eng.*, vol. 55, no. 1, pp. 247–255, Jan. 2008.

[10] M. Sarafianou, A. W. Preece, I. J. Craddock, M. Klemm, and J. A. Leendertz, "Evaluation of two approaches for breast surface measurement applied to a radar-based imaging system," *IEEE Trans. Antennas Propag.*, vol. 64, no. 2, pp. 609–617, Feb. 2016.

[11] K. Noritake and S. Kidera, "Boundary extraction enhanced inverse scattering method for microwave mammography," in *Proc. Eur. Conf. Antennas Propag.*, Apr. 2018, pp. 1–5.

[12] UWCEM, "Numerical breast phantom repository." [Online]. Available: https://uwcem.ece.wisc.edu/phantomRepository.html

[13] R. Pierri, F. Soldovieri, A. Liseno, and F. De Blasio, "Dielectric profiles reconstruction via the quadratic approach in 2-D geometry from multifrequency and multifrequency/multiview data," *IEEE Trans. Geosci. Remote Sens.*, vol. 40, no. 12, pp. 2709–2718, Dec. 2002.

[14] G. Leone, A. Brancaccio, and R. Pierri, "Quadratic distorted approximation for the inverse scattering of dielectric cylinders," *J. Opt. Soc. Amer. A*, vol. 18, no. 3, pp. 600–609, 2001.

[15] S. Kidera, Y. Kani, T. Sakamoto, and T. Sato, "Fast and accurate 3-D imaging algorithm with linear array antennas for UWB pulse radars," *IEICE Trans. Commun.*, vol. E91-B, no. 8, pp. 2683–2691, Aug. 2008.